Available online at www.sciencedirect.com

jmr&t Journal of Materials Research and Technology

www.jmrt.com.br

Original Article

Recycled polypropylene matrix nanocomposites reinforced with silane functionalized geopolymer concrete waste

Flávio James Humberto Tommasini Vieira Ramos[a,*], *Marcelo Henrique Prado da Silva*[b], *Sergio Neves Monteiro*[a], *Andriy Grafov*[c], *Iryna Grafova*[c]

[a] *Instituto de Macromoléculas Professora Eloisa Mano, Universidade Federal do Rio de Janeiro, Avenida Horácio Macedo, 2030-Centro de Tecnologia, Bloco J, Ilha do Fundão, Rio de Janeiro, R.J., 21941 598, Brazil*

[b] *Military Institute of Engineering – IME, Praça General Tibúrcio, 80, Praia Vermelha, Rio de Janeiro, R.J., 22290-270, Brazil*

[c] *University of Helsinki, A.I. Virtasen Aukio 1, PL 55, FI-00014 Helsinki, Finland*

ARTICLE INFO

Article history:
Received 8 July 2019
Accepted 17 April 2020

Keywords:
Geopolymer concrete waste
Recycled polypropylene
Nanocomposite
Silane functionalization
Sustainable material

ABSTRACT

The objective of this work is the processing of recycled polypropylene (rPP) matrix and geopolymer concrete waste (GCW) to develop novel sustainable nanocomposites for engineering applications. Specimens of these nanocomposites were produced from GCW added in proportions of 20, 40 and 50 wt% to rPP. The pulverized waste, with nanometric particles, was used as neat, GCW, or as surface functionalized with vinyl trimethoxy silane (GCW/VTS). Separately, both GCW and GCW/VTS were mixed with rPP by means of extrusion reactive extrusion and injection processing before final molding of specimens. The composition microstructure, thermal stability and tensile properties of the specimens were studied by wide angle X-ray diffraction, thermogravimetry, differential scanning calorimetry, water absorption, tensile tests, and field emission gun scanning electron microscopy with energy dispersive spectroscopy. The main findings were an increased thermal stability and enhanced elastic modulus with incorporation of both GCW and GCW/VTS. A high degree of interaction between GCW filler and rPP matrix, including the first time observed mechanism of PP nanofilaments adhesion, is responsible for a negligible water absorption. A decrease in the crystallinity suggests an interference of GCW in the rPP arrangement of macromolecular chains.

1. Introduction

The worldwide fabrication of cement and concrete is responsible for serious global interferences in the ecosystem and atmosphere, such as destruction of vegetations, land erosion, and high consumption of energy. In addition, the associated CO_2 emissions correspond to about 10% of the total anthropogenic contribution [1–5]. Another significant problem in the production of concrete is the large consumption of water to obtain its amount, or trace, required by the cement. Indeed, the trace is a fundamental parameter in concrete mixture proportion, which influences properties such as setting, strength and durability [6–8]. The standard constitution of a concrete includes aluminosilicates and alite (Ca_3SiO_5), corresponding

* *Corresponding author.*
E-mail: fallmasini1@hotmail.com (F.J. Ramos).

https://doi.org/10.1016/j.jmrt.2020.04.047

to 50–70%, as well as, impurities, such as SiO_2, MgO, Al_2O_3, Fe_2O_3 and some polymorphs like dicalcium silicate (Ca_3SiO_5), tricalcium aluminate ($Ca_3Al_2O_6$) and ferrite (Ca_2AlFeO_5) [9–11].

Recently, the concept of sustainable materials has been highlighted by civil construction industries, through the adoption of mixtures with recycled materials, such as newspaper, honeycomb, agricultural products and polymer wastes for production of eco-friendly concretes [12–14]. Some research works have also been conducted in polymers waste such as the rubber recovered from scrap tires to replace conventional aggregates in the concrete [15–17]. Other polymers, nanoparticles of metal oxides and nanoclays have been considered in the production of high performance concretes. According to [18–21], the nanoparticles permit to increase important properties (thermal, impermeability and mechanicals) of the concrete, and improve new characteristics such as photocatalytic activity, electrical conduction, durability, and reduction of carbon dioxide emissions. Recycled polymers like polyester, vinyl ester, epoxy resins, fibers, polyethylene terephthalate (PET), high density polyethylene and polypropylene (PP) have had success in their incorporation into concrete during manufacture and application [22–25].

Geopolymer is another class of materials gaining considerable attention [26–30] and being extensively used as concrete aggregates [31,19,32,33]. Building structures made of concrete incorporated with geopolymer particles might eventually be demolished and become a waste material. These geopolymer concrete wastes (GCW) have recently become available [34]. Therefore, the objective of the present work is to develop novel composites with GCW, functionalized with vinyl trimethoxy silane (VTS), and incorporated into recycled polypropylene (rPP) by extrusion and injection processes. These composites were characterized and technologically tested.

2. Materials and methods

This work used as basic materials a GCW generated in the production process of construction industry and a rPP from the fabrication of bottles by blow processing. The GCW was supplied as small broken pieces provided by Lafarge LTDA, Brazil, and treated after crushing with 98% purity VTS, supplied by Sigma Aldrich, Brazil. The weight proportions of both GCW and GCW/VTS used to produce the composites were 20, 40 and 50 wt%.

The GCW pieces were first crushed in a Carver hydraulic press, C model, with 18 tones of capacity, in order to reduce the particle size. Then, the crushed material was sieved for analysis of particle size in a Produstest apparatus with an Abronzinox sieve. These sieved particles, most with polyhedral shape and some in the nanometric scale, constitute the neat GCW. The smaller particles (≤270 mesh) were selected to be functionalized with VTS. These selected particles were dispersed in ethanol following sonication for additional disaggregation. After this step, a 0.25 vol% ethanol solution of VTS was poured into the ethanol-dispersed particles and maintained under stirring during 24 h. Then, the dispersion was filtered and washed with ethanol to remove the unreacted silane presented on the surface of the concrete. The next step was to completely dry the silane functionalized geopolymer concrete waste (GCW/VTS) until it reaches constant weight and the samples ready to be processed. The shape of the GCW/VTS particles was mostly as snowflakes.

Pellets of rPP mixed with GCW or GCW/VTS were processed in an extrusion machine, AX 1626 model, SAE 8550 with single steel screw with 16 mm diameter, and four zones of heating. The pellets were processed under four sequence conditions of heating temperature, respectively, at 200, 190, 185 and 180 °C with torque of 60 N m. Next step was the processing of pellets in an injection machine Battenfeld, Plus 35 model.

X-ray diffraction (XRD) analysis was performed in a diffractometer XPert Pro, PANalytical model, with angle 2θ varying from of 5° to 80°. The mode of data acquisition was step width of 0.026° and 400 s/step.

Thermal degradation of precursor materials and composites was evaluated using a TA Instrument Q500 thermogravimetric analyzer. The analysis was carried out from 30 to 700 °C with a rate of 10 °C/min, under nitrogen atmosphere. Initial, maximum rate and final temperatures of the thermal degradation (T_{onset}, T_{max} and T_{end}) were registered. Differential scanning calorimetric (DSC) analyses were carried out using a TA Instruments Q1000 calorimeter. Two thermal cycles were used. In the first, the sample was heated from 0 to 300 °C at 10 °C/min, kept at this temperature for 2 min and then cooled to 0 °C at a maximum scanning rate. A second heating procedure was directly performed from 0 to 300 °C at 10 °C/min. The TG/DTG curves were evaluated in samples of rPP composites reinforced with GCW and with silane functionalization (GCW/VTS) of the concrete surface.

Water absorption test were conducted according to ASTM D570 standard [35] equivalent to ISO 62 (International Organization for Standardization). The samples were analyzed in dried environment under the temperature of 25 °C, after immersion in deionized water during periods of 2 h, 24 h and 6 days following the standard procedures.

The morphologies of the composites, before and after modification, were evaluated by FEI S-4800 field emission scanning electron microscopy (FEG-SEM) with electron beams at 20 kV under vacuum. The sample was placed onto a carbon ribbon and covered with a layer of platinum. The energy dispersive spectroscopy (EDS) analysis was also applied using a Bruker detector to identify and measure the amount of oxides of the geopolymer concrete, and the carbon presence in both the rPP and the silane.

The tensile properties of the rPP and composites were evaluated according to the ASTM D638 standard [36]. The equipment was a model 5569 Instron universal testing machine. Specimens were tensile tested on environment conditions of room temperature (23 °C) and 40% humidity at a strain rate of 2×10^{-4} s^{-1}. The results compared specimens of both functionalized geopolymer concrete (GCW/VTS) and neat GCW incorporated rPP composites.

3. Results and discussion

XRD of rPP from used bottles is shown in Fig. 1(a). The peaks at 14.3°, 17°, 18.8° and 22° were attributed to planes (1 1 0), (0 4 0), (1 3 0), (1 1 1) of the monoclinic crystals of iPP (isotactic polypropylene) in α-phase. Trigonal crystals in

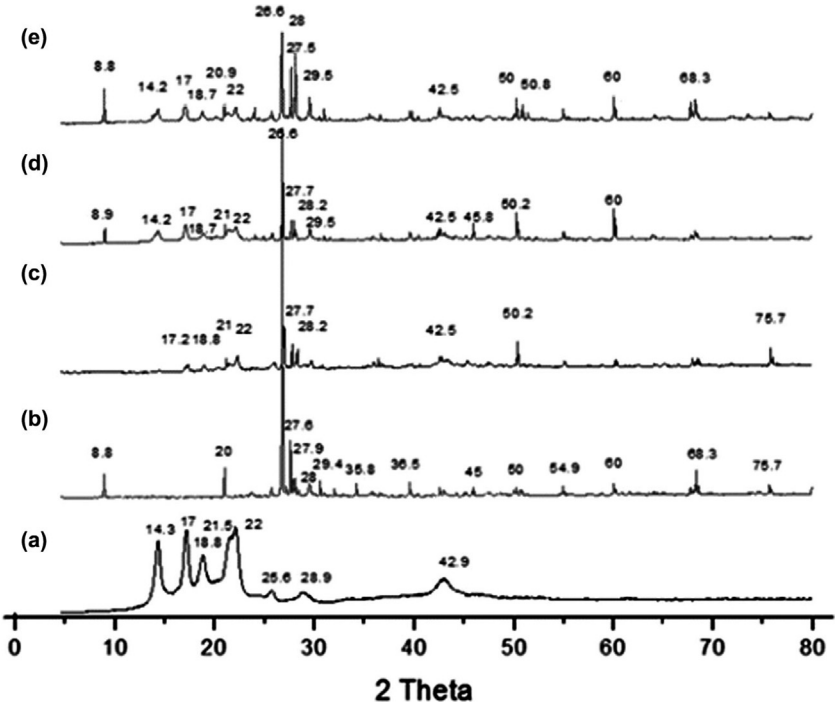

Fig. 1 – X-ray diffractogram of: (a) rPP; (b) rPP composite with neat GCW; (c) rPP composite with 20 wt% of GCW functionalized with VTS; (d) rPP composite with 40 wt% GCW/VTS; and (d) rPP composite with 50 wt% GCW/VTS.

β-phase were also presented at the angle 21.4° corresponding to the reflection of the (3 0 1) plane. Reflections at 25.6° and 28.9° were considered corresponding to (0 6 0) and (2 2 0) of α-phase [22,37,38]. While reflection at 42.9° can be attributed to the filler industrially used to increase the polydispersion of polypropylene during the blow processing of the recycled bottles. Through the amorphous halo was possible to observe two contributions (amorphous and crystalline) in the rPP corresponding to the variation of the orientation and intensities characteristics of a recycled material [1,24].

According to Fig. 1(b) the XRD analysis of the GCW detected the crystallinity structures and shows representative peaks of different minerals, such as alite ($3CaO{\cdot}SiO_2$), belite ($2CaO{\cdot}SiO_2$), aluminate ($3CaO{\cdot}Al_2O_3$) and calcium aluminoferrite – $Ca_2(Al,Fe)_2O_5$. Alite, the major phase presented in approximately 50–70%, is constituted by some impurities such as MgO, Al_2O_3, and Fe_2O_3 as well as some polymorphs [2,39]. The peaks related to alite (Ca_3SiO_5) were observed at $2\theta = 32°$, 33.4° and 41°. The other component, belite (Ca_2SiO_4) was associated with peaks at $2\theta = 26°$, 28°, 31°, 34°, 41°, 44.5°, 45.5°, 56°, 57° and 59° [40], calcium carbonate ($CaCO_3$) observed at $2\theta = 3.85°$ and 2.49° and dolomite $CaMg(CO_3)_2$ observed at $2\theta = 2.40°$, 1.81° and 1.79°. A relatively low amount of aluminates was associated with peaks at $2\theta = 46°$ and 60°. The calcium aluminoferrite was detected at $2\theta = 50°$ [30,31]. Other peaks were assigned to magnesium oxide at $2\theta = 37°$, 62° and 78°, calcium carbonate at $2\theta = 8.7°$, 21°, 23°, 29°, 36°, 39°, 47° and 78° and calcium hydroxide at $2\theta = 18°$, 37°, 41°, 46° and 47° [2,40]. Indeed, the presence of several forms of aluminosilicates and other compositions of ceramic materials evidence the crystalline phases of the silane functionalized GCW composites.

TGA results of thermal degradation and its derivative DTG for rPP, as well as neat GCW and silane functionalized GCW/VTS composites are shown in Figs. 2–4. The TG/DTG curves for rPP in Fig. 2 as well as composites with neat GCW in Fig. 3; and composites with silane functionalized GCW/VTS in Fig. 4, display prominent levels of mass loss as well as related onset (T_{onset}), maximum rate (T_{max}) and end (T_{end}) thermal temperatures.

Table 1 presents the T_{onset}, T_{max}, T_{end}, and residue of the samples. According to results in this table, the temperatures of all rPP matrix composites incorporated with GCW and GCW/VTS are displaced to higher degradation temperatures compared to plain rPP. Furthermore, among the composites, there is a tendency of increasing T_{onset} with the amount of incorporated GCW. This apparently indicates that the GCW contributes to improve the thermal stability of the rPP polymeric structure. This will be further discussed. Other interesting fact can be observed in the rPP–50 GCW/VTS, which during degradation produced lower residue 40% as compared with the rPP–50 GCW. This might be attributed to the superior structural stability provided by the silane functionalization. The similar T_{end}, found at 483 °C, on the other hand, indicates comparable chemical interaction between GCW fillers and polymer matrix, independent of silane functionalization. This interaction corresponds to a mechanism of nanometric adhesion between rPP filaments and GCW particles further identified in SEM images.

Fig. 5 shows that the DSC curves of the composites with geopolymer silane functionalized concrete waste (GCW/VTS) display the same profile of the composites with neat GCW. The curves of both composites show two exothermic events at 126 °C and 157 °C. These different temperatures were

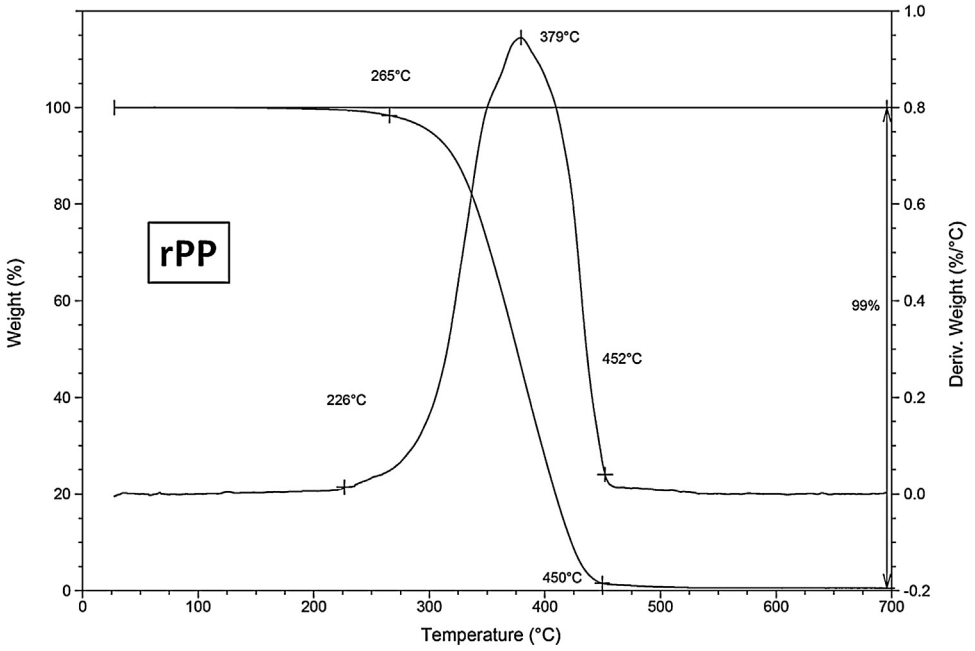

Fig. 2 – TG/DTG curves of rPP.

Table 1 – Onset (T_{onset}), maximum rate (T_{max}), end (T_{end}) temperatures and residues (wt%) from thermogravimetric analyses of rPP and its composites with neat GCW or silane functionalized GCW/VTS.

Samples	T_{onset} (°C)	T_{max} (°C)	T_{end} (°C)	Residue (%)
rPP	265	379	452	1
rPP–20 GCW	391	462	489	13
rPP–40 GCW	398	462	483	40
rPP–50 GCW	411	464	483	53
rPP–20 GCW/VTS	340	459	493	23
rPP–40 GCW/VTS	379	462	485	36
rPP–50 GCW/VTS	369	460	483	40

attributed to melting point of polypropylene crystals – β and α, respectively, by Zhou et al. [22]. They demonstrated this difference in a research work about different crystallization behavior of olefin block copolymer in α and β polypropylene matrix. As such, within the interval of temperature investigated by the DSC analysis, the incorporated GCW, either neat or silane functionalized, did not interfere with the composite thermal behavior.

In spite of the thermal inertness of GCW within the DSC temperature interval in Fig. 5, its incorporation in the composite affects the crystallinity of the rPP matrix. In Table 2, it is presented the crystallinity degree of the rPP as well as those of both composites incorporated with neat GCW and silane functionalized GCW/VTS. Similar to the results of the neat (GCW) hybrid composites, the GCW/VTS composites reveal a decrease of the crystallinity degree with higher proportions of GCW filler. This suggests that the incorporation of GCW modifies the structural arrangements of the macromolecular chains of the rPP toward a more heterogeneous (less crystalline) configuration.

Table 2 – Crystallinity degree, X_c%, of rPP and its composites with neat GCW or silane functionalized GCW/VTS.

Samples	X_c (%)
rPP	37.94
rPP–20 GCW	34.87
rPP–40 GCW	26.66
rPP–50 GCW	10.76
rPP–20 GCW/VTS	33.33
rPP–40 GCW/VTS	21.53
rPP–50 GCW/VTS	20.51

An analysis of water absorption was performed to quantify the amount of water absorbed by the composites. Results contributed to the understanding of the relationships between microstructures, thermal and mechanical properties. According to these results presented in Table 3, not only the rPP but also its composites incorporated with neat GCW or GCW with VTS, has negligible water absorption. Possibly this effect occurred due to the formation of a polymeric coating around the concrete particles after the injection processing, as it was observed in the FEG-SEM analysis. Table 3 shows that the values of water absorption were bellow the detection limit of 0.01% for the different composites.

Microscopy analysis in Fig. 6 revealed the morphology of rPP and GCW particles as well as the processed composites. The morphology of plain rPP, Fig. 6(a), is composed of large

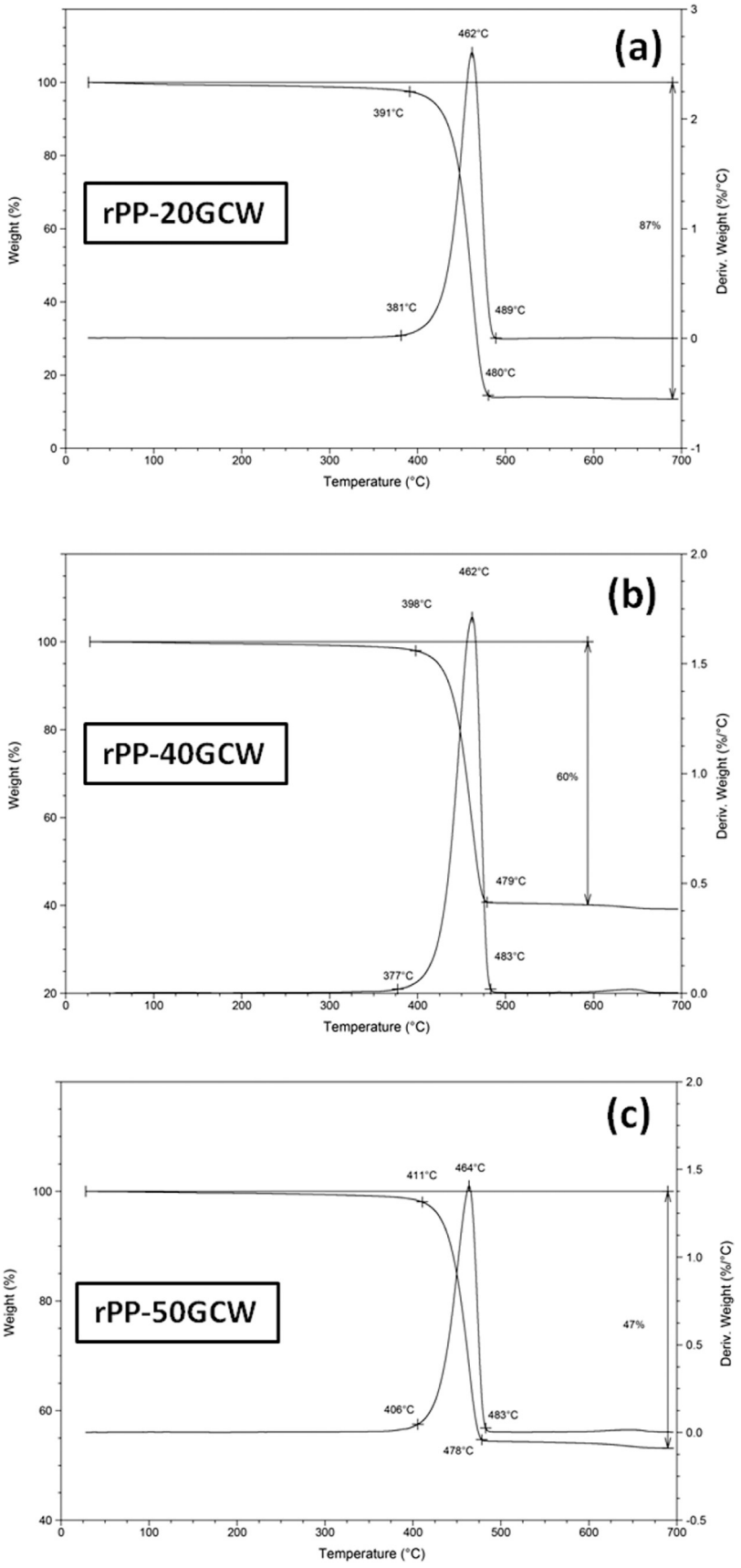

Fig. 3 – TG/DTG curves of rPP matrix composites incorporated with: (a) 20 wt%; (b) 40 wt%; and (c) 50 wt% of neat GCW.

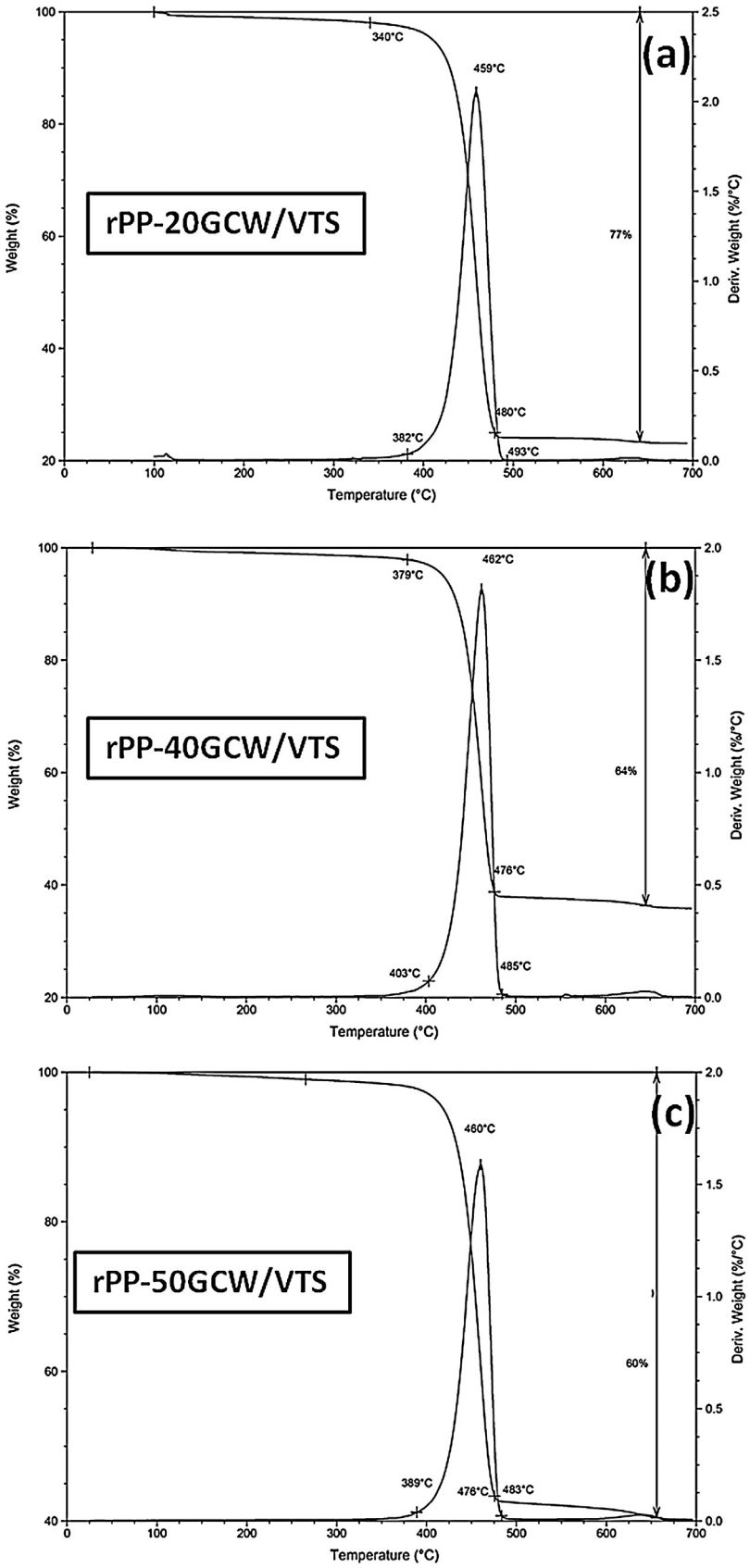

Fig. 4 – TG/DTG curves of rPP matrix composites incorporated with: (a) 20 wt%; (b) 40 wt%; and (c) 50 wt% of silane functionalized geopolymer concrete waste (GCW/VTS).

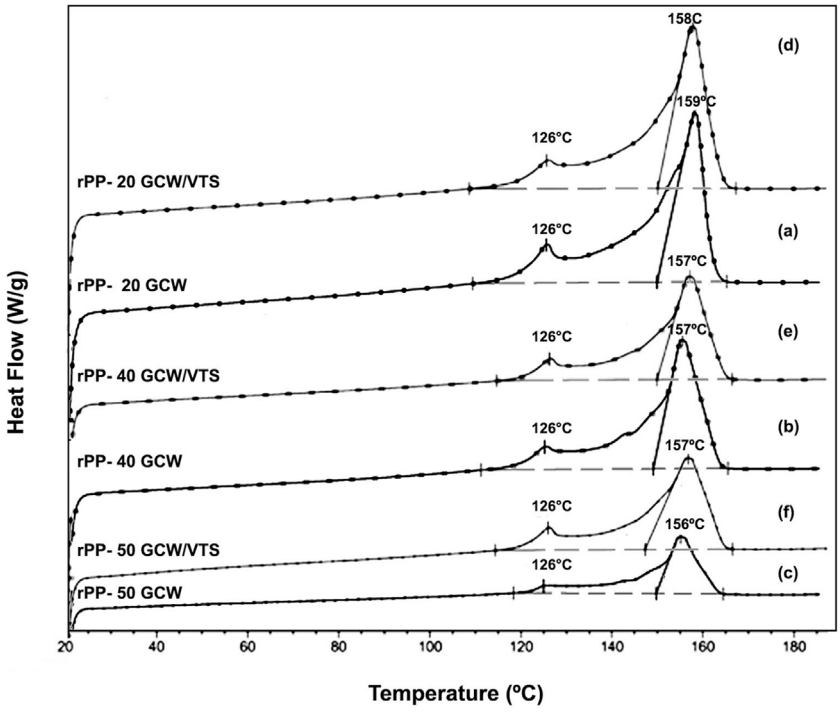

Fig. 5 – DSC curves of rPP matrix composites incorporated with: (a) 20 wt%; (b) 40 wt%; and (c) 50 wt% GCW as well as (d) 20 wt%; (e) 40 wt%; and (f) 50 wt% VTS functionalized GCW/VTS.

Table 3 – Water absorption [35] of rPP and its composites with neat GCW or silane functionalized GCW/VTS.

Sample	Water absorption (%)
rPP	≤0.01
rPP–20 GCW	≤0.01
rPP–40 GCW	≤0.01
rPP–50 GCW	≤0.01
rPP–20 GCW/VTS	≤0.01
rPP–40 GCW/VTS	≤0.01
rPP–50 GCW/VTS	≤0.01

continuous smooth regions without evidence of distinct phases, although polypropylene is known to have two phases [22]. The neat GCW in Fig. 6(b) display an agglomerate of small polyhedral particles, some of them in the nanometric scale. Incorporation of these GCW particles, either neat or functionalized GCW/VTS, into rPP matrix produced composites with micro and nanostructures shown in Figs. 6(c) and (d). In most cases, the incorporation of either GCW or GCW/VTS occurs as non-homogeneous dispersion of agglomerated particles, like in Fig. 6(g). With higher magnification, as in the insert of Fig. 7, it is for the first time observed a mechanism of adhesion between the mineral GCW particles and polymeric matrix by means of polypropylene nanofilaments. These rPP nanofilaments might be responsible for the effective adhesion between matrix and filler in the composites. Moreover, the nanometric particles of GCW, disclosed in some pictures in Fig. 6, as well as the rPP nanofilaments in Fig. 7 would permit the denomination of nanocomposite. Therefore, it is suggested that these nanostructural characteristic, for the first time revealed in rPP matrix composites incorporated with GCW or GCW/VTS, could contribute to the negligible water absorption in Table 3 and tensile results further presented in this work.

EDS analysis was performed at several points of the FEG-SEM images, mainly those associated with polyhedral particles supposedly of GCW. Fig. 8 illustrates a typical EDS analysis and corresponding related chemical composition. With the exception of Pt sputtered in the samples for electrical conductivity, the elements Mg, Al, K, Ti, Mn and Fe confirmed the GCW nature of the particle analyzed. While the Si, C and O are possibly confirming the silane functionalization.

The tensile properties of the rPP and its composites with neat GCW or silane functionalized GCW/VTS are presented in Table 4. In this table the first point to be emphasized is that the incorporation of GCW, both neat and silane functionalized, decreased the strength of the rPP matrix. Similar decrease occurs for the total strain. However, the stiffness of all composites, given by the elastic modulus, are improved. This reinforcement is particularly significant in the case of 50 wt.% incorporation of GCW and GCW/VTS. The apparent contradiction between decrease in strength and increase in stiffness is due to the brittle and harder nature of the GCW, as compared to the more flexible and softer rPP. Brittle particles of GCW promote premature fracture in the composites while contributing to a stiffer linear elastic behavior.

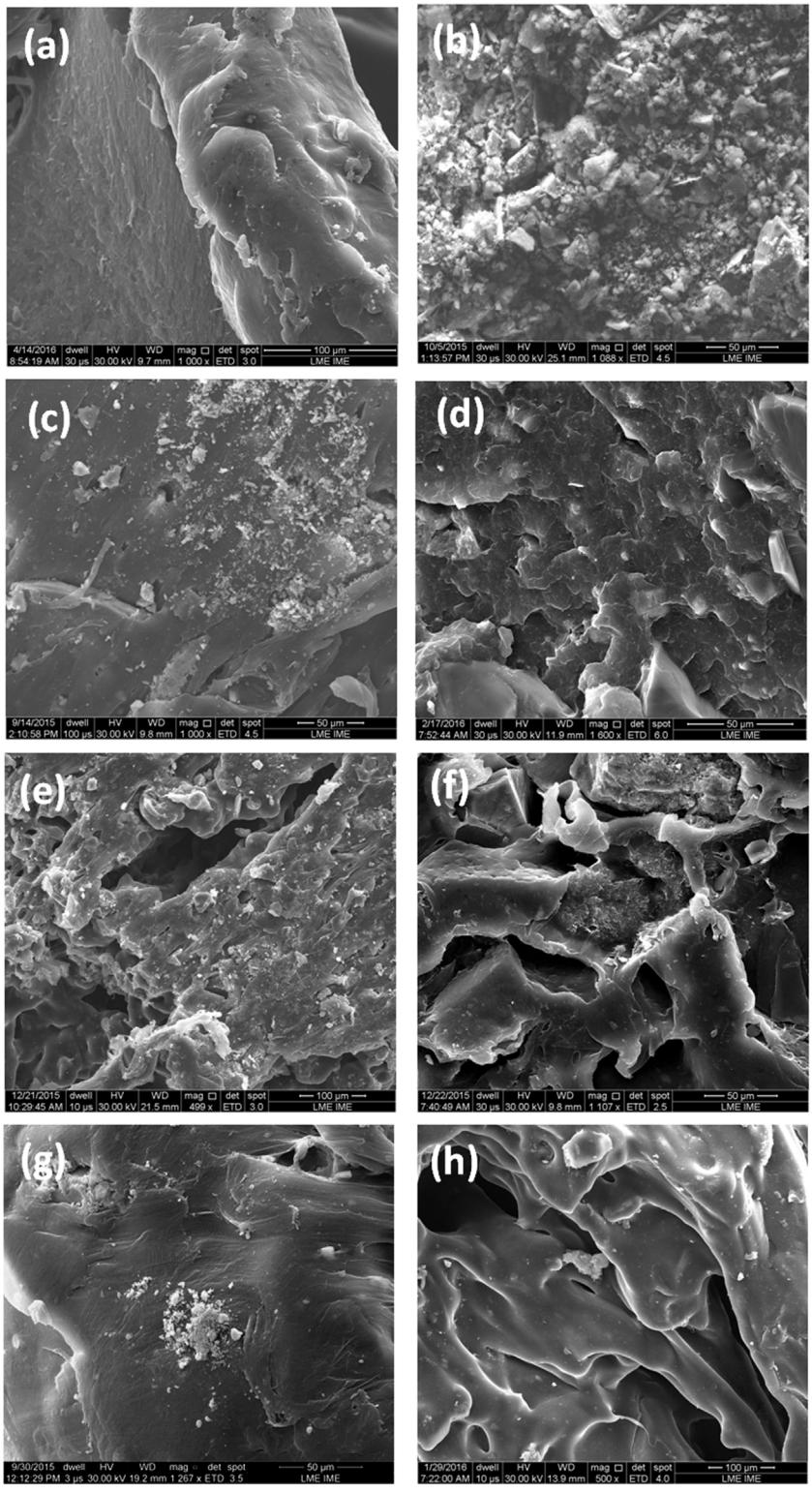

Fig. 6 – SEM micrographs of: (a) rPP; (b) neat GCW; (c) rPP composite with 20 wt% GCW; (d) rPP composite with 40 wt% GCW; (e) rPP composite with 50 wt% GCW; (f) rPP composite with 20 wt% of GCW functionalized with VTS; (g) rPP composite with 40 wt% GCW/VTS; and (h) rPP composite with 50 wt% GCW/VTS.

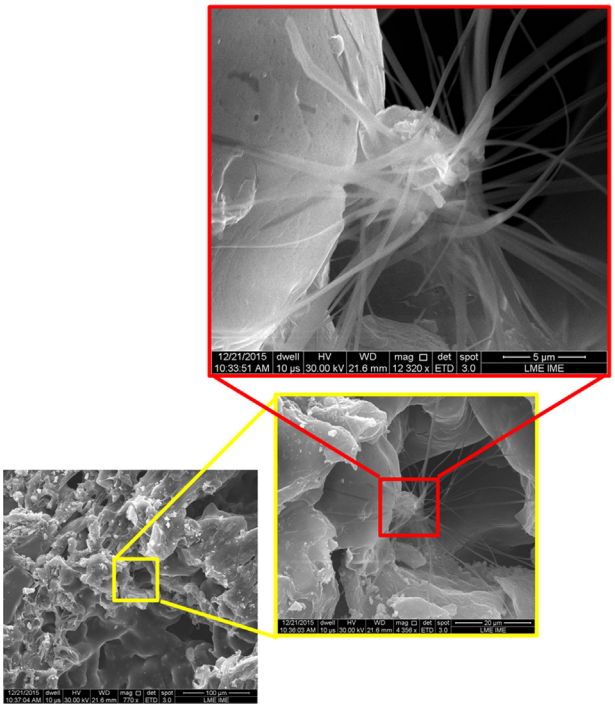

Fig. 7 – SEM micrographs of rPP matrix composite incorporated with 50 wt% GCW/VTS. Insert showing organic nanofilaments participating in the adhesion between matrix and filler.

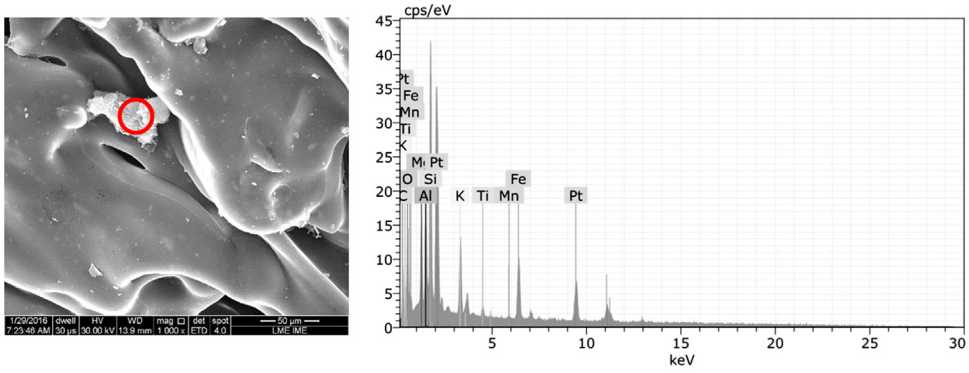

C	O	Mg	Al	Si	K	Ti	Mn	Fe	Pt
19.1	19.6	2.52	1.89	8.57	2.64	1.19	0.25	7.54	36.7

Fig. 8 – EDS analysis at a GCW/VTS particle and corresponding semi-quantitative chemical composition.

Table 4 – Tensile properties [36] of rPP and its composites with neat GCW or silane functionalized GCW/VTS.

Samples	Tensile stress at maximum load (MPa)	Uniform strain at maximum load (%)	Tensile stress at break (MPa)	Total strain at break (%)	Young's modulus (MPa)
rPP	34.63	13.69	31.94	17.95	643.90
rPP–20 GCW	27.62	10.11	22.87	14.52	652.21
rPP–40 GCW	23.18	5.73	21.43	9.12	856.39
rPP–50 GCW	19.99	5.03	19.44	5.62	865.38
rPP–20 GCW VTS	29.91	8.89	26.80	12.32	653.82
rPP–40 GCW VTS	26.61	7.41	23.68	9.95	696.68
rPP–50 GCW VTS	30.23	5.73	29.88	5.94	920.46

4. Conclusions

- A study on sustainable nanocomposites of rPP matrix incorporated with GCW both neat or VTS functionalized, revealed significant changes compared to the polymer matrix characteristics.
- TG/DTG showed an increase of the thermal stability for all nanocomposites. This can be assigned to the effective interaction between matrix and dispersed fillers, such as the formation of rPP connecting nanofilaments.
- DSC analysis exhibited a decrease in the crystallinity degree (X_c) with the amount of incorporated GCW. These changes were related the influence of the GCW (neat and functionalized) during crystallization of the rPP matrix.
- A negligible water absorption obtained for plain rPP and all nanocomposites is attributed to the encapsulation of geopolymer concrete particles by the polymeric matrix, with the contribution of nanofilaments.
- Structural analyses by FEG-SEM showed smooth rPP and small polyhedral particles of GCW, some in the nanometric scale. Incorporation of both neat GCW and GCW/VTS occurs as a dispersion of agglomerated particles. For the first time is observed a mechanism of filler adhesion to a polymer matrix by polypropylene nanofilaments.
- EDS analysis associated with GCW/VTS particles indicates the chemical composition of elements including Si and C that might be possibly related to VTS.
- Tensile test results disclosed a decrease in both strength and strain with incorporation of GCW or GCW/VTS in the rPP. However the elastic modulus is significantly improved. This is ascribed to the comparatively brittle and harder GCW causing premature fracture in the composites while contributing to a stiffer elastic behavior.

Conflict of interest

The authors declare no conflicts of interest.

Uncited reference

[41].

Acknowledgments

The authors thank the Brazilian supporting agencies CNPq, CAPES, FAPERJ for the funding.

REFERENCES

[1] Scarfato P, Di Maio L, Fariello ML, Russo P, Incarnato L. Preparation and evaluation of polymer/clay nanocomposite surface treatments for concrete durability enhancement. Cement Concr Compos 2012;34:297–305.
[2] Sabai MM, Cox MGDM, Mato RR, Egmond ELC, Lichtenberg JJN. Concrete block production from construction and demolition waste in Tanzania. Resour Conserv Recycl 2013;72:9–19.
[3] Xue J, Shinozuka M. Rubberized concrete: A green structural material with enhanced energy-dissipation capability. Constr Build Mater 2013;42:196–204.
[4] Becchio C, Corgnati SP, Kindinis A, Pagliolico S. Improving environmental sustainability of concrete products: investigation on MWC thermal and mechanical properties. Energy Build 2009;41:1127–34.
[5] Zhang T, Gao P, Gao P, Wei J, Yu Q. Effectiveness of novel and traditional methods to incorporate industrial wastes in cementitious materials – an overview. Resour Conserv Recycl 2013;74:134–43.
[6] Ganesan N, Raj JB, Shashikala AP. Flexural fatigue behavior of self compacting rubberized concrete. Constr Build Mater 2013;44:7–14.
[7] Mo L, Panesar DK. Effects of accelerated carbonation on the microstructure of Portland cement pastes containing reactive MgO. Cem Concr Res 2012;42:769–77.
[8] Zhang Z, Provis JL, Reid A, Wanga H. Geopolymer foam concrete: an emerging material for sustainable construction. Constr Build Mater 2014;56:113–27.
[9] Zivica V, Palou MT, Bagel L, Krizma M. Low-porosity tricalcium aluminate hardened paste. Constr Build Mater 2013;38:1191–8.
[10] Emanuelson A, Hansen S, Viggh E. A comparative study of ordinary and mineralised Portland cement clinker from two different production units. Part I: Composition and hydration of the clinkers. Cem Concr Res 2003;33:1613–21.
[11] Shtepenko O, Hills C, Brough A, Thomas M. The effect of carbon dioxide on dicalcium silicate and Portland cement. Chem Eng J 2006;118:107–18.
[12] Vivian WY, Gao TXF, Tama CM. Microstructural analysis of recycled aggregate concrete produced from two-stage mixing approach. Cem Concr Res 2005;35:1195–203.
[13] Bosque IFS, Ramírez SM, Varela MTB. FTIR study of the effect of temperature and nanosilica on the nanostructure of C–S–H gel formed by hydrating tricalcium silicate. Constr Build Mater 2014;52:314–23.
[14] Herrera AD, Juárez CA, Valdez P, Bentz DP. Evaluation of sustainable high-volume fly ash concretes. Cement Concr Compos 2011;33:39–45.
[15] Faustino J, Pereira L, Soares S, Cruz D, Paiva A, Varum H, et al. Impact sound insulation technique using corncob particleboard. Constr Build Mater 2012;37:153–9.
[16] Aiello MA, Leuzzi F. Waste tyre rubberized concrete: properties at fresh and hardened state. Waste Manage 2010;30:1696–704.
[17] Tayeb MMA, Bakar BHA, Ismail H, Akil HM. Effect of partial replacement of sand by recycled fine crumb rubber on the performance of hybrid rubberized-normal concrete under impact load: experiment and simulation. J Cleaner Prod 2013;59:284–9.
[18] Hanus MJ, Harris AT. Nanotechnology innovations for the construction industry. Prog Mater Sci 2013;58:1056–102.
[19] Mukharjee BB, Barai SV. Influence of nano-Silica on the properties of recycled aggregate concrete. Constr Build Mater 2014;55:29–37.
[20] Sua-iam G, Makul N. Use of recycled alumina as fine aggregate replacement in self-compacting concrete. Constr Build Mater 2013;47:701–10.
[21] Chen J, Poon C-S. Photocatalytic activity of titanium dioxide modified concrete materials – influence of utilizing recycled glass cullets as aggregates. J Environ Manage 2009;90:3436–42.
[22] Zhou X, Feng J, Cheng D, Yi J, Wang L. Different crystallization behavior of olefin block copolymer in α-and β-polypropylene matrix. Polymer 2013;54:4719–27.
[23] Sawpan MA, Mamun AA, Holdsworth PG. Long term durability of pultruded polymer composite rebar in concrete environment. Mater Des 2014;57:616–24.

[24] Wang N, Ellinwood BR. Estimating nominal strength of built-up CFRP laminates from standardized specimen tests. Struct Saf 2014;47:24–8.
[25] Mahdi F, Abbas H, Khan AA. Flexural, shear and bond strength of polymer concrete utilizing recycled resin obtained from post consumer PET bottles. Constr Build Mater 2013;44:798–811.
[26] Petlitckaia S, Poulesquen A. Design of lightweight metakaolin based geopolymer formed with hydrogen peroxide. Ceramic Int 2019;45:1322–30.
[27] Mucsi G, Szenczi A, Nagy S. Fiber reinforced geopolymer from synergetic utilization of fly ash and waste tire. J Cleaner Prod 2018;178:429–40.
[28] Kioupis D, Kavakakis C, Tsivilis S, Kakali G. Synthesis and characterization of porous fly ash-based geopolymers using Si as foaming agent. Adv Mater Sci Eng 2018, http://dx.doi.org/10.1155/2018/1942898.
[29] Onutai S, Jiemsirilers S, Thavorniti P, Kobayashi T. Fast microwave syntheses of fly ash based porous geopolymers in the presence of high alkali concentration. Ceram Int 2016;42:9866–74.
[30] Mohseni E, Kazemi MJ, Koushkbaghi M, Zehtab B, Behforouz B. Evaluation of mechanical and durability properties of fiber-reinforced lightweight geopolymer composites based on rice husk ash and nano-alumina. Constr Build Mater 2019;209:532–40.
[31] Zadeh VD, Bobko CP. Nanoscale mechanical properties of concrete containing blast furnace slag and fly ash before and after thermal damage. Cement Concr Compos 2013;37:215–21.
[32] Karthik A, Sudalaimani K, Vijayakumar CT. Durability study on coal fly ash-blast furnace slag geopolymer concretes with bio-additives. Ceram Int 2017;43:11935–43.
[33] Hamdi N, Messaoud IB, Srasra E. Production of geopolymer binders using clay minerals and industrial wastes. Comptes Rendus Chimie 2019;22:220–6.
[34] Ramos FJHTV, Reis RHM, Grafova I, Grafov A, Monteiro SN. Eco-friendly recycled polypropylene matrix composites incorporated with geopolymer concrete waste particles. J Mater Res Technol 2020, http://dx.doi.org/10.1016/j.jmrt.2020.01.054.
[35] American Society for Testing Materials. ASTM D570-98. Standard test method for water absorption of plastics. West Conshohocken, PA: ASTM; 2010.
[36] American Society for Testing Materials. ASTM D638-14, standard test method for tensile properties of plastics. West Conshohocken, PA: ASTM; 2015.
[37] Sampaio EMV, Filho ACR. The WAXD and tensile stress and elongation at the yield point of polypropylene additive films. Macromolecula Symposia 2007;245-246:123–8.
[38] Machado G, Denardin ELG, Kinast TEJ, Gonçalves MC, Luca MA, Teixeira SR, et al. Crystalline properties and morphological changes in plastically deformed isotatic polypropylene evaluated by X-ray diffraction and transmission electron microscopy. Eur Polym J 2005;41:129–38.
[39] Wongkeo W, Thogsanitgarn P, Pimraksa K, Chaipanich A. Compressive strength, flexural strength and thermal conductivity of autoclaved concrete block made using bottom ash as cement replacement materials. Mater Des 2012;35:434–9.
[40] Mymrin V, Correa SM. New construction material from concrete production and demolition wastes and lime production waste. Constr Build Mater 2007;21:578–82.
[41] Lee TC, Lin KL, Su XW, Lin KK. Recycling CMP sludge as a resource in concrete. Constr Build Mater 2012;30:243–51.